

Correlations between mass, stellar kinematics and gas metallicity in EAGLE galaxies

L. J. Zenocratti,^{1*} M. E. De Rossi,^{2,3†} M. A. Lara-López,⁴ T. Theuns⁵

¹Facultad de Ciencias Astronómicas y Geofísicas, Universidad Nacional de La Plata, Paseo del Bosque s/n, B1900FWA, La Plata, Argentina

²Universidad de Buenos Aires, Facultad de Ciencias Exactas y Naturales y Ciclo Básico Común. Buenos Aires, Argentina

³CONICET-Universidad de Buenos Aires, Instituto de Astronomía y Física del Espacio (IAFE). Buenos Aires, Argentina

⁴DARK, Niels Bohr Institute, University of Copenhagen, Lyngbyvej 2, Copenhagen DK-2100, Denmark

⁵Institute for Computational Cosmology, Physics Department, University of Durham, South Road, Durham DH1 3LE, UK

Accepted XXX. Received YYY; in original form ZZZ

ABSTRACT

The metallicity of star-forming gas in galaxies from the EAGLE simulations increases with stellar mass. Here we investigate whether the scatter around this relation correlates with morphology and/or stellar kinematics. At redshift $z = 0$, galaxies with more rotational support have lower metallicities on average when the stellar mass is below $M_{\star} \approx 10^{10} M_{\odot}$. This trend inverts at higher values of M_{\star} , when prolate galaxies show typically lower metallicity. At increasing redshifts, the trend between rotational support and metallicity becomes weaker at low stellar mass but more pronounced at high stellar mass. We argue that the secondary dependence of metallicity on stellar kinematics is another manifestation of the observed anti-correlation between metallicity and star formation rate at a given stellar mass. At low masses, such trends seem to be driven by the different star-formation histories of galaxies and stellar feedback. At high masses, feedback from active galactic nuclei and galaxy mergers play a dominant role.

Key words: galaxies: abundances - galaxies: evolution - galaxies: high-redshift - galaxies: star formation - cosmology: theory.

1 INTRODUCTION

The relation between stellar mass and gas-phase metallicity in galaxies (henceforth the mass-metallicity relation, MZR) has been studied extensively in the last decades from both an observational (Tremonti et al. 2004; Lara-López et al. 2010) and a theoretical (Calura et al. 2009; Yates et al. 2012; De Rossi et al. 2015; De Rossi et al. 2017-hereafter, DR17; Sharma & Theuns 2019) point of view. At redshift $z \sim 0$, gas metallicity, Z , increases with stellar mass, M_{\star} , approximately as a power-law, $Z \propto M_{\star}^{2/5}$; the slope of the correlation flattens towards higher masses. This power-law trend is also seen at higher redshifts, though possibly with a different slope and normalisation (e.g. Troncoso et al. 2014).

The scatter along the observed MZR correlates with other properties of galaxies. Ellison et al. (2008) showed that, at given stellar mass, observed galaxies with smaller half-mass radii or lower specific star formation rates (sSFR) tend to have higher gas metallicity, as quantified by the oxygen abundance, O/H. To account for these observations,

Lara-López et al. (2010) and Mannucci et al. (2010) suggested the existence of a three-dimensional relation between M_{\star} , O/H and star formation rate (SFR), where systems with higher SFRs tend to have lower O/H at a given value of M_{\star} . Alternatively, this 3D relation could result from a more fundamental underlying relation between M_{\star} , O/H and *gas fraction* (f_{g}), since f_{g} and SFR correlate (e.g. Bothwell et al. 2013, Lara-López et al. 2013). Deciding which relation is more fundamental could be helped by examining other correlations. Recent observations suggest that Z tends to be lower in galaxies with a higher concentration, higher Sérsic index, or higher SFR (Wu et al. 2019), at given value of M_{\star} . Unfortunately, surprisingly large uncertainties remain in inferring physical relations from the data because different methods yield significantly different answers (e.g. Telford et al. 2016). In fact, some observational studies do not find that the scatter around the MZR correlates with SFR (e.g. Sánchez et al. 2019), and some studies claim that the correlation exists but inverts at high M_{\star} (e.g. Yates et al. 2012).

In this paper we examine the scatter around the MZR in galaxies from the EAGLE cosmological hydrodynamical simulations (Schaye et al. 2015). The ‘Evolution and Assembly of

* E-mail: ljenocratti@hotmail.com

† E-mail: mariaemilia.dr@gmail.com

GaLaxies and their Environments’ (EAGLE) suite of cosmological hydrodynamical simulations uses sub-grid models calibrated to reproduce a small set of observations at $z \approx 0$, as described in [Crain et al. \(2015\)](#). The simulations then reproduce a relatively extensive set of other observations, including the evolution of the galaxy stellar mass function ([Furlong et al. 2015](#)), of galaxy sizes ([Furlong et al. 2017](#)), of optical ([Trayford et al. 2015](#)) and UV and IR luminosities ([Camps et al. 2018](#)). DR17 analysed the secondary metallicity dependencies in EAGLE (including the dependencies on SFR, sSFR, f_g and stellar age, t_*), obtaining good agreement with observed trends (see also [Lara-López et al. 2019](#)). In particular, DR17 show that EAGLE galaxies follow remarkably well the observed ‘Fundamental Metallicity Relation’ introduced by [Mannucci et al. \(2010\)](#). In addition, [Sánchez Almeida & Dalla Vecchia \(2018\)](#) show that EAGLE simulations are able to reproduce the observed secondary metallicity dependence on the size of galaxies.

In this Letter, we report new predictions of EAGLE simulations regarding the connection between MZR scatter and internal morpho-kinematics of galaxies. Such trends were not previously reported in MZR studies. In a forthcoming article, we address the origin of these metallicity secondary dependencies by analysing the formation histories of different galaxy populations. This Letter is organized as follows. In Section 2, we briefly describe the EAGLE simulations and the galaxy selection criteria. In Section 3, we analyse the simulated MZR as a function of the morphology and kinematics of the galaxies. We discuss the origin of our obtained trends in Section 4. We summarise our findings in Section 5.

2 THE EAGLE SIMULATIONS

A full description of the EAGLE simulation suite is given by [Schaye et al. \(2015\)](#). Briefly, the suite was simulated with the GADGET-3 incarnation of the TREEPM-SPH code described by [Springel \(2005\)](#), with sub-grid modules for physics whose parameters are calibrated to reproduce the $z \approx 0$ galaxy stellar mass function, the relation between galaxy mass and size, and the black hole mass - stellar mass relation ([Crain et al. 2015](#)). The adopted cosmological parameters are taken from [Planck Collaboration \(2015\)](#): $\Omega_\Lambda = 0.693$, $\Omega_m = 0.307$, $\Omega_b = 0.04825$, $n_s = 0.9611$, $Y = 0.248$, and $h = 0.677$.

EAGLE consists of simulations with various box sizes and particle masses. Here, we mainly use simulation labelled ‘Ref-L100N1504’ in [Schaye et al. \(2015\)](#), which has a co-moving extent of $L = 100$ co-moving megaparsecs (cMpc) and a baryonic particle mass of $\sim 1.2 \times 10^6 M_\odot$ (corresponding to 1504^3 particles). We have verified that the main trends and conclusions presented in this work are consistent with those from the higher-resolution EAGLE simulation ‘Recal-L025N0752’, analysed previously by DR17.

EAGLE galaxies are identified using a combination of the ‘friends-of-friends’ (FOF) and SUBFIND algorithms. This picks-out ‘self-bound’ structures of gas, stars and dark matter. Here we analyse the properties of both central galaxies (the dominant galaxies in FOF halos) and satellites¹. Following DR17, we measure baryonic properties within spherical

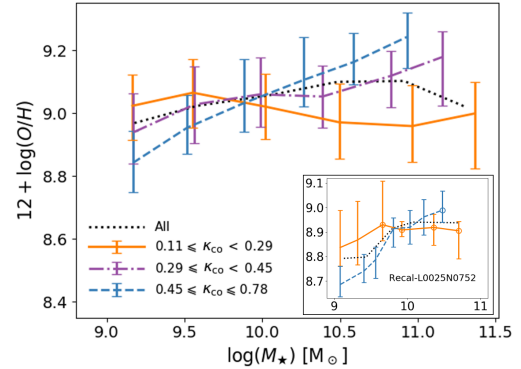


Figure 1. *Black dotted line:* median M_* - O/H (MZR) relation in redshift $z = 0$ EAGLE galaxies from simulation Ref-L100N1504. *Coloured lines:* MZR relation for EAGLE galaxies binned by κ_{co} , the fraction of stellar kinetic energy in rotation: the lowest third κ_{co} (orange), intermediate κ_{co} (purple) and the highest third κ_{co} (blue). Error bars encompass the 25th and 75th percentiles. *Inset:* as main panel, but for the higher resolution EAGLE simulation Recal-L0025N0752.

apertures of 30 proper kilo-parsecs (pkpc) and characterize the ‘metallicity’ of star-forming gas by its O/H abundance (EAGLE tracks 11 abundances, including oxygen and hydrogen). We analyse galaxies with at least 25 star-forming gas particles (gas mass at least $5.25 \times 10^7 M_\odot$) which we found to be a reasonable compromise between numerical resolution and bias. To characterize the stellar morphology and kinematics, we use the fraction of kinetic energy in co-rotation, κ_{co} , the disc-to-total stellar mass ratio, D/T , the ratio V/σ of stellar rotation to velocity dispersion, the ellipticity, ϵ_* , of the stellar body, and its triaxiality, T . These were computed by [Thob et al. \(2019\)](#) and can be queried in the EAGLE database² ([McAlpine et al. 2016](#); [The EAGLE team 2017](#)).

3 CORRELATING MORPHOLOGY AND METALLICITY

EAGLE’s $z = 0$ MZR is plotted in Fig. 1, with galaxies binned by κ_{co} , the fraction of stellar kinetic energy of the galaxy that is invested in ordered rotation. Below $M_* \sim 10^{10} M_\odot$, dispersion-supported galaxies (low κ_{co} , orange line) have higher O/H than rotationally supported galaxies (blue line) of the same M_* . Also striking is that O/H increases with M_* for rotationally supported galaxies, but is almost independent of M_* for dispersion-supported galaxies. As a consequence, the trend between O/H and κ_{co} inverts above $M_* \approx 10^{10} M_\odot$, with massive dispersion-supported galaxies having *lower* O/H than rotationally supported galaxies of the same mass. We find similar trends in the higher resolution simulation Recal-L025N0752 (inset of Fig. 1).

The results of Fig. 1, combined with the dependence of O/H on the SFR, sSFR and the gas fraction reported by DR17, suggest that κ_{co} may itself correlate with these other galaxy parameters. We examine this in Fig. 2. Independent of M_* , the gas fraction (middle panel) and the specific star formation rate (right panel) both increase with κ_{co} , being

¹ Our main results are unchanged if we analyse only centrals.

² <http://eagle.strw.leidenuniv.nl>, <http://www.eaglesim.org/>

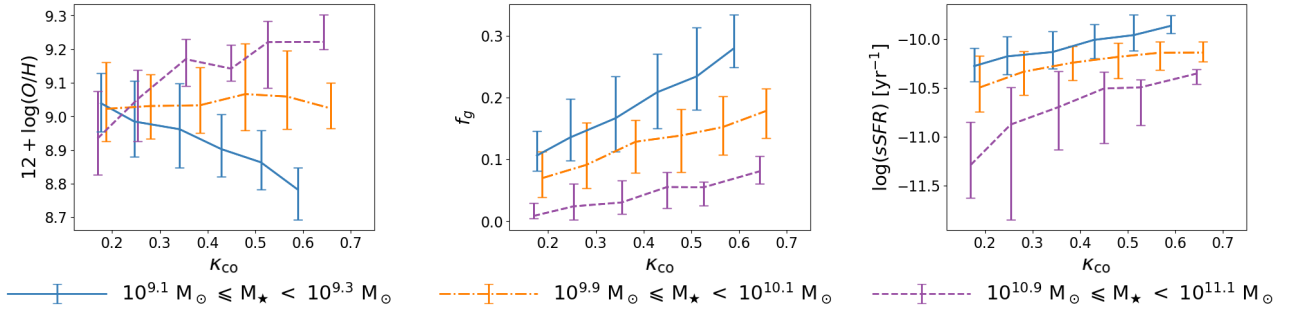


Figure 2. Correlation between O/H (left panel), gas fraction f_g (middle panel), and the specific star formation rate (right panel) and κ_{co} , the fraction of stellar kinetic energy in rotation, for $z = 0$ EAGLE galaxies from simulation Ref-L100N1504. Galaxies are binned in stellar mass: low stellar mass (blue), intermediate stellar mass (orange) and high stellar mass (purple), see legend. Curves represent the median relation, error bars encompass the 25th and 75th percentiles.

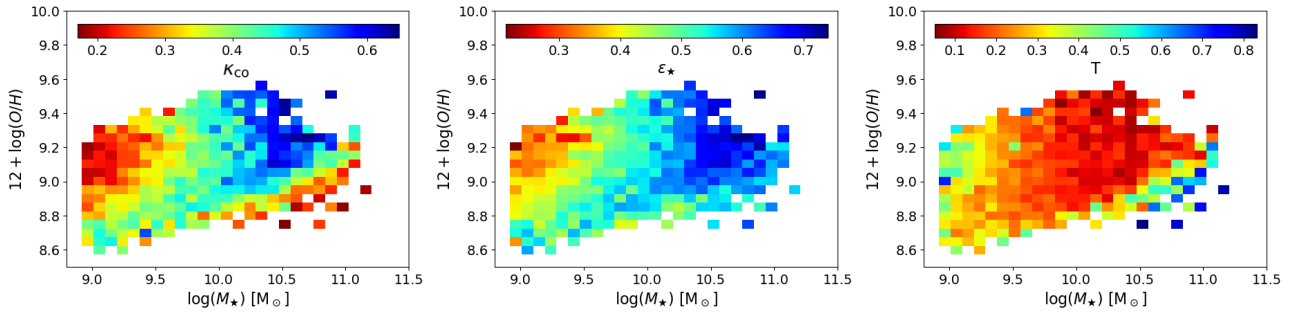


Figure 3. O/H metallicity as a function of stellar mass, M_{\star} , for $z = 0$ EAGLE galaxies from simulation Ref-L100N1504. Bins in O/H- M_{\star} are coloured according to the median value of κ_{co} (left panel), the stellar ellipticity ϵ_{\star} (middle panel) and the galaxy's triaxiality parameter T (right panel).

the increase of f_g the most pronounced for the lower M_{\star} galaxies (blue line), whereas the increase of the sSFR is more evident in the *higher* M_{\star} galaxies (purple line). The sSFR is a measure of the rate at which metals are produced, and f_g a measure of the size of the reservoir that dilutes those metals. Therefore, a consequence of these trends is that O/H *decreases* with increasing κ_{co} at low M_{\star} , whereas it *increases* for high mass galaxies (see left panel); at $M_{\star} \sim 10^{10} M_{\odot}$, O/H does not depend on κ_{co} . These findings are consistent with the relation between colour and kinematics of EAGLE galaxies studied by Correa et al. (2017). Our results are also consistent with the observations by Calvi et al. (2018) that late-type galaxies have higher SFR and sSFR compared to S0 and elliptical galaxies of the same mass.

How these correlations arise is analysed in more detail³ in Fig. 3. At $M_{\star} < 10^{10} M_{\odot}$, galaxies typically have low κ_{co} , but there is a tail of galaxies with high κ_{co} and low O/H: this tail generates the anti-correlation between κ_{co} and O/H in Fig. 2. These outliers are also gas-rich and have unusually high stellar ellipticities, ϵ_{\star} , and low triaxiality parameter T . At $M_{\star} > 10^{10} M_{\odot}$, galaxies have usually a high value of κ_{co} , but now there is a tail of galaxies with low κ_{co} and high T that are typically more massive and have low O/H. At intermediate masses, $M_{\star} \sim 10^{10} M_{\odot}$, there is relatively little variation in κ_{co} or ϵ_{\star} .

³ Similar results are obtained if using D/T or V/σ instead of κ_{co} .

We plot the MZR relation at different redshifts z in the left panel of Fig. 4. At a given z , the sample of simulated galaxies is separated in two sub-samples, using the median value of κ_{co} ($\bar{\kappa}_{\text{co}}$) at that z . Note that the value of $\bar{\kappa}_{\text{co}}$ tends to decrease with increasing z : dispersion-supported galaxies increasingly dominate at higher z . As expected, the normalization of the MZR decreases with z , with such evolution being independent of κ_{co} at $M_{\star} \sim 10^{10} M_{\odot}$. As we also noticed at $z = 0$, there is a clear increase of O/H with M_{\star} for galaxies with high κ_{co} , but this trend is mostly absent for the low κ_{co} galaxies. At the low-mass end ($M_{\star} \lesssim 10^{10} M_{\odot}$), the secondary dependence of O/H on κ_{co} tends to vanish as z increases, due mainly to an increase of the MZR slope for systems with $\kappa_{\text{co}} < \bar{\kappa}_{\text{co}}$ at $z \gtrsim 1$. On the other hand, at high masses ($M_{\star} \gtrsim 10^{10} M_{\odot}$), the secondary dependence of O/H on κ_{co} tends to be stronger at higher z , which, in this case, is caused by an increase of the MZR slope for systems with $\kappa_{\text{co}} > \bar{\kappa}_{\text{co}}$ at $z \gtrsim 2$. Similar evolutionary trends are obtained when using other morpho-kinematical indicators.

4 DISCUSSION

Reproducing observed metallicity scaling relations is an important test of current cosmological hydrodynamical simulations, with many of them showing good agreement with observations (e.g., DR17, Davé et al. 2019; Torrey et al. 2019).

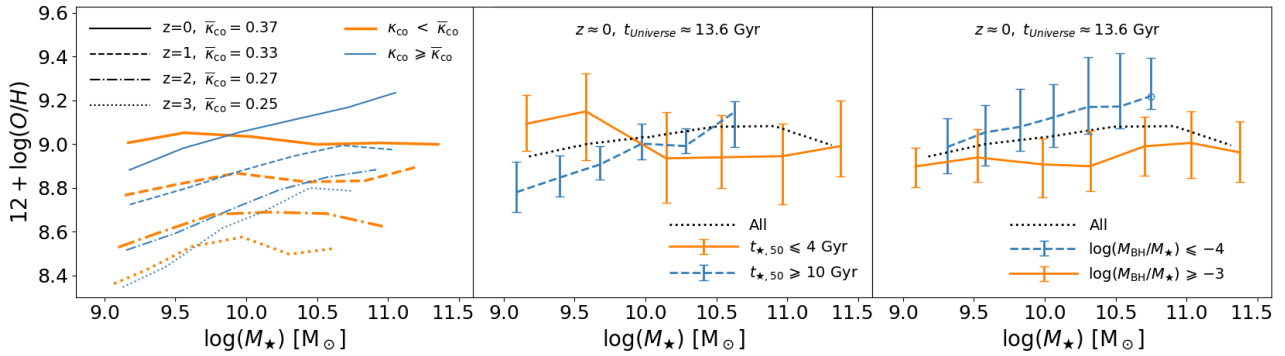


Figure 4. Left panel: MZR at different z , as indicated in the figure. Curves representing galaxies with rotational support below the median at the given z are plotted in *thick orange*, those with higher κ_{co} are plotted in *thin blue*. Middle and right panels: $z = 0$ MZR binned according to $t_{*,50}$ (the time when galaxies reached half of their present M_*) and M_{BH}/M_* (the BH-stellar mass ratio), respectively.

In this context, metal-poor gas inflows have been suggested to play a key role on driving secondary O/H dependences (at a given mass) on galaxy sizes (e.g. [Sánchez Almeida & Dalla Vecchia 2018](#)), SFRs and gas fractions (e.g. DR17).

In addition, [Torrey et al. \(2018\)](#) claimed that similar evolution timescales of SFR and O/H may be required to explain the O/H- M_* -SFR relation in the *Illustris-TNG* simulations. For more massive galaxies, mergers and AGNs might also play a crucial role on shaping the MZR (e.g. DR17, [Ma et al. 2016](#)). Although different works have focused on the O/H dependence on SFR, its relation with morphokinematics has not been discussed before. As a consistency check, we analysed the dependence of MZR on morphokinematics in the *Illustris-TNG* simulations, obtaining similar general trends to those shown in Fig. 1: at low masses, galaxies with higher D/T ratios generally have lower O/H, and the opposite is true for more massive systems. Hence, generally, such trends seem to be robust against the details of physical implementations adopted in these models. Nevertheless, we highlight that the detailed features of metallicity scaling relations (e.g. detailed shape, scatter and normalization) do depend on the different model prescriptions; this work is focused on predictions from the *EAGLE* model.

[Calura et al. \(2009\)](#) analysed the MZR of galaxies using ‘chemical evolution’ models. They did not find a clear dependence of O/H on morphology at a given mass and z , which might be a consequence of the different assumptions made in their models. For example, they assume that galaxies retain the same morphology throughout their evolution and they neglect mergers. In contrast in the *EAGLE* simulations, discs may be destroyed during mergers and may re-grow following accretion ([Trayford et al. 2019](#)).

In the middle panel of Fig. 4, we show the *EAGLE* $z = 0$ MZR binned according to the cosmic time, $t_{*,50}$, when galaxies reached half of their present stellar mass, M_* . At the low-mass end, systems with lower O/H tend to have been formed at later times. These systems also show higher sSFRs, higher gas fractions and lower stellar ages (DR17), exhibiting also higher rotational support and disky morphologies (Fig. 1 and 3). An analysis of the formation histories of these galaxies suggests that such trends would be associated with the accumulated effects of accretion of metal-poor gas at *late* times (generally, $z \lesssim 1$), which dilutes the metal content of galax-

ies, triggers their star formation activity and contributes to the formation of the galaxy disc.⁴ This is consistent with the left panel of Fig. 4, which shows that the dependence of the low-mass MZR on κ_{co} is more significant towards $z = 0$.

The right panel of Fig. 4 shows the MZR binned according to the black hole-stellar mass ratio (M_{BH}/M_*). Massive galaxies with higher M_{BH}/M_* tend to have lower O/H. This is consistent with the results of DR17, who claimed that AGNs quench the metallicity evolution of galaxies by heating the gas, suppressing the star formation activity and ejecting metals out of the systems. Thus, at the high-mass end, less metal-enriched systems have lower sSFRs, lower fraction of star-forming gas and higher ages. Such systems tend also to be dispersion-supported, on average (Fig. 1 and 3). A preliminary analysis of the merger histories of *EAGLE* galaxies suggests that massive galaxies with lower O/H seem to have been subjected to major mergers events, which inhibited the formation of a disc and also contributed to the increase of the central BH mass. The analysis of the formation histories of *EAGLE* galaxies and its connection to the scatter of the MZR will be the subject of a forthcoming article ([Zenocratti et al., in prep.](#)).

[Sharma & Theuns \(2019\)](#) propose a model of self-regulated galaxy formation, in which the star formation rate, stellar mass, gas mass and metallicity depend on halo mass, cosmological accretion rate and redshift, but regulated by feedback. In their ‘ $\Gamma\kappa\epsilon\alpha$ ’ model, the main astrophysical parameter ϵ is a dimensionless measure of the efficiency of stellar feedback: a large value of ϵ implies efficient feedback and low star formation rate, while feedback is inefficient and the star formation rate is high for a small ϵ . This leads to the following scaling for Z and f_g with M_* and efficiency ϵ :

$$Z \propto \frac{M_*^{2/5}}{\epsilon^{3/5}}; \quad f_g \propto \frac{\epsilon^{\frac{2}{5} \frac{n-1}{n}}}{M_*^{\frac{3}{5} \frac{n-1}{n}}} \approx \frac{\epsilon^{0.11}}{M_*^{0.17}}, \quad (1)$$

where $n \approx 1.4$ is the slope of the Kennicutt-Schmidt star formation law. These relations show that when feedback is efficient (meaning ϵ is large, $\epsilon \approx 1$), Z is low and f_g is high,

⁴ Long-term gas accretion could occur continuously or by successive gas inflow events.

whereas on the other hand, inefficient feedback ($\epsilon \ll 1$) implies Z is high and f_g low. We can connect this to the morphology of the galaxy by speculating that feedback in a thin disc - corresponding to a galaxy with high κ_{co} - is more efficient than when κ_{co} is low (a more spheroidal gas distribution). High-resolution simulations that resolve individual supernova energy injections in gas columns suggest this type of relation between feedback efficiency and disc morphology. For example, the simulations by Creasey et al. (2013) show that supernova explosions that occur above or below the disc are more efficient at driving winds, because cooling losses are suppressed when the explosion occurs at the lower densities that prevail there (see also Girichidis et al. 2016). Thus, in EAGLE, accretion of metal-poor gas seems to trigger the formation of a disc but, once the disc has already been formed, feedback effects would play a role on regulating the subsequent metallicity evolution. We leave the analysis of feedback effects on EAGLE disk galaxies for a future work.

5 CONCLUSIONS

We analysed the stellar mass-gas metallicity relation (MZR) as function of morpho-kinematical parameters in the EAGLE cosmological hydrodynamical simulations. At $z = 0$, we found new secondary dependencies of metallicity on the internal kinematics and morphology of galaxies. At low masses ($M_* \lesssim 10^{10} M_\odot$), higher metallicities are found for more spheroidal and lower rotation-supported galaxies.

A preliminary analysis of the star formation histories of low-mass galaxies indicate that late accretion of metal-poor gas dilutes the metal content of galaxies, triggers their star formation activity and contributes to the formation of the galaxy disc. When the gas is in a thin, rotationally supported disc, feedback may be more efficient, which results in lower O/H and a higher gas fraction (Sharma & Theuns 2019). The trends in more massive galaxies are generally less strong, with lower metallicities found in more prolate galaxies with lower levels of rotational support. AGN feedback and mergers seem to play a key role on shaping the MZR at the high-mass end. At increasing redshifts, the trend between rotational support and metallicity becomes weaker at low stellar mass but more pronounced at high stellar mass. These trends are consistent with the secondary dependencies of O/H (at a fixed mass) on gas fraction, star formation rate and stellar age, and the relation between the latter quantities with galaxy morpho-kinematics (see DR17).

Our findings regarding the O/H secondary dependencies (at fixed stellar mass) on morpho-kinematics and their relation with the scatter of the MZR were not previously discussed in the literature. A detailed analysis of the origin and evolution of the Mass-Metallicity-Morpho-kinematics Relation in EAGLE will be presented in a future article.

ACKNOWLEDGEMENTS

LJZ and MEDR acknowledge support from PICT-2015-3125 of ANPCyT, PIP 112- 201501-00447 of CONICET and UNLP G151 of UNLP (Argentina). MALL is a DARK-Carlsberg Foundation Fellow (Semper Ardens project CF15-0384). We acknowledge the Virgo Consortium for making

their simulation data available. The EAGLE simulations were performed using the DiRAC-2 facility at Durham, managed by the ICC, and the PRACE facility Curie based in France at TGCC, CEA, Bruyères-le-Châtel. This work used the DiRAC@Durham facility managed by the Institute for Computational Cosmology on behalf of the STFC DiRAC HPC Facility (www.dirac.ac.uk). The equipment was funded by BEIS capital funding via STFC capital grants ST/P002293/1, ST/R002371/1 and ST/S002502/1, Durham University and STFC operations grant ST/R000832/1. DiRAC is part of the National e-Infrastructure.

REFERENCES

- Bothwell M. S., Maiolino R., Kennicutt R., Cresci G., Mannucci F., Marconi A., Ciccone C., 2013, *MNRAS*, **433**, 1425
- Calura F., Pipino A., Chiappini C., Matteucci F., Maiolino R., 2009, *A&A*, **504**, 373
- Calvi R., Vulcani B., Poggianti B. M., Moretti A., Fritz J., Fasano G., 2018, *MNRAS*, **481**, 3456
- Camps P., et al., 2018, *ApJS*, **234**, 20
- Correa C. A., et al., 2017, *MNRAS*, **472**, L45
- Crain R. A., et al., 2015, *MNRAS*, **450**, 1937
- Creasey P., Theuns T., Bower R. G., 2013, *MNRAS*, **429**, 1922
- Davé R., Anglés-Alcázar D., Narayanan D., Li Q., Rafieferantsoa M. H., Appleby S., 2019, *MNRAS*, **486**, 2827
- De Rossi M. E., Theuns T., Font A. S., McCarthy I. G., 2015, *MNRAS*, **452**, 486
- De Rossi M. E., Bower R. G., Font A. S., Schaye J., Theuns T., 2017, *MNRAS*, **472**, 3354
- Ellison S. L., Patton D. R., Simard L., McConnachie A. W., 2008, *ApJ*, **672**, L107
- Furlong M., et al., 2015, *MNRAS*, **450**, 4486
- Furlong M., et al., 2017, *MNRAS*, **465**, 722
- Girichidis P., et al., 2016, *MNRAS*, **456**, 3432
- Lara-López M. A., et al., 2010, *A&A*, **521**, L53
- Lara-López M. A., et al., 2013, *MNRAS*, **433**, L35
- Lara-López M. A., De Rossi M. E., Pilyugin L. S., Gallazzi A., Hughes T. M., Zinchenko I. A., 2019, *MNRAS*, **490**, 868
- Ma X., et al., 2016, *MNRAS*, **456**, 2140
- Mannucci F., Cresci G., Maiolino R., Marconi A., Gnerucci A., 2010, *MNRAS*, **408**, 2115
- McAlpine S., et al., 2016, *Astronomy and Computing*, **15**, 72
- Planck Collaboration 2015, *A&A*, **594**, A13
- Sánchez Almeida J., Dalla Vecchia C., 2018, *ApJ*, **859**, 109
- Sánchez S. F., et al., 2019, *MNRAS*, **484**, 3042
- Schaye J., et al., 2015, *MNRAS*, **446**, 521
- Sharma M., Theuns T., 2019, arXiv e-prints, p. arXiv:1906.10135
- Springel V., 2005, *MNRAS*, **364**, 1105
- Telford O. G., Dalcanton J. J., Skillman E. D., Conroy C., 2016, *ApJ*, **827**, 35
- The EAGLE team 2017, ArXiv e-prints: 1706.09899,
- Thob A. C. R., et al., 2019, *MNRAS*, **485**, 972
- Torrey P., et al., 2018, *MNRAS*, **477**, L16
- Torrey P., et al., 2019, *MNRAS*, **484**, 5587
- Trayford J. W., et al., 2015, *MNRAS*, **452**, 2879
- Trayford J. W., Frenk C. S., Theuns T., Schaye J., Correa C., 2019, *MNRAS*, **483**, 744
- Tremonti C. A., et al., 2004, *ApJ*, **613**, 898
- Troncoso P., et al., 2014, *A&A*, **563**, A58
- Wu Y.-Z., Zhang W., Zhao Y.-H., 2019, *MNRAS*, **486**, 5310
- Yates R. M., Kauffmann G., Guo Q., 2012, *MNRAS*, **422**, 215

This paper has been typeset from a $\text{\TeX}/\text{\LaTeX}$ file prepared by the author.